Simulations of Concentrated Suspensions of Semirigid Fibers: Effect of Bending on the Rotational Diffusivity

Philip D. Cobb and Jason E. Butler*

Department of Chemical Engineering, The University of Florida, Gainesville, Florida 32611-6005

Received October 6, 2005; Revised Manuscript Received November 9, 2005

ABSTRACT: Brownian dynamics simulations of the behavior of semirigid polymers demonstrate that small deviations from rigid models affect the dynamics of rod suspensions and that the dynamics are sensitive to the hydrodynamic model. Simulations were performed with two models having different short-time diffusivities. The first was a slender-body dimer model, where two rigid slender-bodies are joined at their ends, and the second was a three-bead trimer model where the beads are connected by rigid rods. A potential was applied to hinder the bending of the rods. An aspect ratio (rod length over diameter) of 50 was used for all simulations, and an excluded volume potential was used to prevent the rods from crossing one another. Simulations of systems of stiff rods which are not quite rigid show a delayed onset of semidilute behavior in comparison to simulations of rigid rod systems, with different hydrodynamic models providing different power-law scalings of the rotational diffusivities within the semidilute concentration regime.

1. Introduction

Recent computer simulations[1] have demonstrated that the choice of model used to represent individual rods within a concentrated suspension of rigid rods with excluded volume interactions substantially impacts the rotational dynamics. The key difference is the distribution of the hydrodynamic resistance along the rods which alters the ratio of the short-time diffusivities, $L^2D_{R_0}/D_{T_0}$, where L is the total length of the rod, and D_{R_0} and D_{T_0} are the rotational and average center of mass diffusivities of a single rod at infinite dilution. The rotational diffusivity has been theorized to have a power-law scaling in the semidilute regime of $D_R/D_{R_0} \sim (nL^3)^{\nu}$.[2−4] Cobb and Butler[1] showed that ν can be as low as -2 in agreement with the simulations and theories of Doi,[2] can equal -1 in agreement with other work by Fixman[3,4] and Bitsanis et al.,[5,6] and ranges from any value between approximately -0.2 and -2 depending on the ratio of $L^2D_{R_0}/D_{T_0}$ for the model used in the simulation.

Small deviations from perfect rigidity have also been cited as having a significant impact on the dynamics of rod suspensions.[7−9] Experiments on fibers of poly(γ-benzyl-*L*-glutamate) (PBLG) suspended in *m*-cresol[10] have been cited many times as a model system for suspensions of rigid rods.[5,6,11,12] However, recent criticisms have raised questions about whether the results of the experiments performed by Mori et al.[10] should be compared to the results of simulations of rigid rods since PBLG may not be completely rigid.[9,13,14] Cush and Russo[9] claim that flexibility in the PBLG polymer, especially near the ends of the fibers, causes a difference in the results in comparison to rigid rods.

The simulations performed here used two simple models to investigate the dual role of slight bending and choice of model on the dynamics of concentrated systems of semirigid rods. The small deviations from rigidity delay the onset of semidilute behavior in suspensions of rods, while the choice of model results in different power-law scalings in the semidilute to concentrated regime. The methods used to perform simulations are discussed in section 2. The results of the simulations are then presented in section 3, and the discussion and conclusions based on these results are in sections 4 and 5.

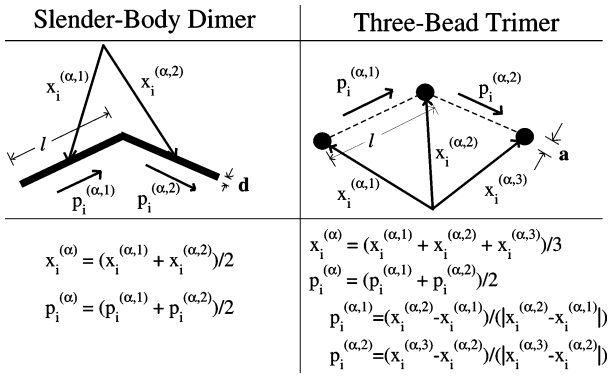

Figure 1. Two models of the semirigid rods used in the simulations, where l is the length of each individual segment of the rod, d is the diameter of the slender-body dimer model, and a is the diameter of each bead in the three-bead trimer model. Also included are the equations for calculating the overall center of mass position $x_i^{(\alpha)}$ and orientation $p_i^{(\alpha)}$ of rod α based on the positions and orientations of each component.

2. Simulation Method

In the simulations performed here, two different models were used for the rods as shown in Figure 1. The first model is a dimer composed of two slender-bodies,[15,16] and the second is a trimer composed of three beads.[17] Both models are composed of two rigid segments connected by constraints, similar to the "once-broken rod" model.[18] A bending force is applied which hinders the bending of the rods. For a high bending force, the slender-body dimer behaves as a rigid slender-body, having a value of $L^2D_{R_0}/D_{T_0} = 9$ and $D_{\|_0}/D_{\perp_0} = 2$,[19−21] where $D_{\|_0}$ is the diffusivity in the direction parallel to the central rod axis at infinite dilution, and $D_{\perp_0}$ is the diffusivity in the direction perpendicular to the central rod axis at infinite dilution. The three-bead trimer behaves as a rigid trimer when a high bending force is applied, having $L^2D_{R_0}/D_{T_0} = 6$ and $D_{\|_0}/D_{\perp 0} = 1$.

The center of mass position $x_i^{(\alpha)}$ of each rod is calculated by averaging the center of mass positions of each segment of the

* Corresponding author. E-mail: butler@che.ufl.edu.

10.1021/ma052164b CCC: $33.50
Published on Web 12/16/2005

rod. The slender-body dimer model is composed of two segments each with a center of mass, $x_i^{(\alpha,1)}$ and $x_i^{(\alpha,2)}$. The three-bead trimer model is composed of three beads with centers at $x_i^{(\alpha,1)}$, $x_i^{(\alpha,2)}$, and $x_i^{(\alpha,3)}$. The unit vector $p_i^{(\alpha)}$ defines the overall orientation of rod α, which is calculated by averaging the two individual segment orientations, $p_i^{(\alpha,1)}$ and $p_i^{(\alpha,2)}$. For the three-bead trimer model, the orientation of each of the two segments is calculated by taking the difference between the center of mass positions of the two beads on the segment (beads 1 and 2 for segment 1 and beads 2 and 3 for segment 2) divided by the magnitude of the distance (l) between them.

2.1. Governing Equations. The dynamics of each rod is given by the Langevin equations without inertia

$$\xi_{ij}^{(\alpha)}\dot{r}_j^{(\alpha)} = \mathscr{F}_i^{(\alpha,\mathrm{Br})} + \mathscr{F}_i^{(\alpha,\mathrm{Ev})} + \mathscr{F}_i^{(\alpha,\mathrm{Bend})} + \mathscr{F}_i^{(\alpha,\mathrm{Const})} + \mathscr{F}_i^{(\alpha,\mathrm{Corr})} \quad (1)$$

where $\xi_{ij}^{(\alpha)}$ is the hydrodynamic resistance matrix of rod α and $\dot{r}_i^{(\alpha)}$ is a vector containing the center of mass and rotational velocities of rod α. For the slender-body dimer model the vector $\dot{r}_j^{(\alpha)}$ is defined as

$$\dot{r}_j^{(\alpha)} = [\dot{x}_i^{(\alpha,1)}, \dot{x}_i^{(\alpha,2)}, \dot{p}_i^{(\alpha,1)}, \dot{p}_i^{(\alpha,2)}] \quad (2)$$

where j has a length of 12, i has a length of 3, $\dot{x}_i^{(\alpha,1)}$ and $\dot{x}_i^{(\alpha,2)}$ are the center of mass velocities of segments 1 and 2 of rod α, and $\dot{p}_i^{(\alpha,1)}$ and $\dot{p}_i^{(\alpha,2)}$ are the rotational velocities of each of the two segments. For the three-bead trimer model the vector $\dot{r}_j^{(\alpha)}$ is defined as

$$\dot{r}_j^{(\alpha)} = [\dot{x}_i^{(\alpha,1)}, \dot{x}_i^{(\alpha,2)}, \dot{x}_i^{(\alpha,3)}] \quad (3)$$

where j has a length of 9, and $\dot{x}_i^{(\alpha,1)}$, $\dot{x}_i^{(\alpha,2)}$, and $\dot{x}_i^{(\alpha,3)}$ are the center of mass velocities of the three beads. The terms $\mathscr{F}_i^{(\alpha,\mathrm{Br})}$, $\mathscr{F}_i^{(\alpha,\mathrm{Ev})}$, $\mathscr{F}_i^{(\alpha,\mathrm{Bend})}$, $\mathscr{F}_i^{(\alpha,\mathrm{Const})}$, and $\mathscr{F}_i^{(\alpha,\mathrm{Corr})}$ are the Brownian, excluded volume, bending, constraint, and correction forces and torques acting on each segment of rod α. Each force vector is then defined for the slender-body model as

$$\mathscr{F}_j^{(\alpha,*)} = [F_i^{(\alpha,1)}, F_i^{(\alpha,2)}, \tilde{F}_i^{(\alpha,1)}, \tilde{F}_i^{(\alpha,2)}] \quad (4)$$

and for the three-bead dimer model as

$$\mathscr{F}_j^{(\alpha,*)} = [F_i^{(\alpha,1)}, F_i^{(\alpha,2)}, F_i^{(\alpha,3)}] \quad (5)$$

where the indices i and j have the same values as those for the velocity vectors in eqs 2 and 3, and the * indicates the type of force or torque being applied (Br, Ev, Bend, Const, or Corr as in eq 1). The forces on the centers of mass of the slender-bodies and the beads of the three-bead dimer models are given by F_i, and the torques (weighted forces[1]) are given by $\tilde{F}_i$.

2.2. Evaluation of Brownian Forces. The fluctuating Brownian forces satisfying the fluctuation dissipation theorem have a mean of zero,

$$\left\langle \mathscr{F}_i^{(\alpha,\mathrm{Br})} \right\rangle = 0 \quad (6)$$

and a variance of

$$\left\langle \mathscr{F}_i^{(\alpha,\mathrm{Br})} \mathscr{F}_j^{(\alpha,\mathrm{Br})} \right\rangle = 2k_\mathrm{B}T\xi_{ij}^{(\alpha)}\delta(t-t') \quad (7)$$

where $k_\mathrm{B}T$ is the thermal energy and $\delta(t-t')$ is the Dirac δ function. These simulations use unprojected Brownian forces,[15,16,22] unlike other approaches[17] where the Brownian forces are initially projected orthogonal to the constraints. The Brownian forces are given by

$$\mathscr{F}_i^{(\alpha,\mathrm{Br})} = \mathscr{B}_{ij}^{(\alpha)} w_j^{(\alpha)} \quad (8)$$

where $w_j^{(\alpha)}$ is a random vector of length 12 for the slender-body dimer model and 9 for the three-bead trimer model for each rod α. The vector $w_j^{(\alpha)}$ has the properties of

$$\left\langle w_i^{(\alpha)} \right\rangle = 0, \quad \text{and} \quad \left\langle w_i^{(\alpha)} w_j^{(\alpha)} \right\rangle = \delta_{ij} \quad (9)$$

The matrix $\mathscr{B}_{ij}^{(\alpha)}$ is related to the resistance matrix through the relation

$$\mathscr{B}_{\mathrm{ik}}^{(\alpha)} \mathscr{B}_{\mathrm{jk}}^{(\alpha)} = \frac{2k_\mathrm{B}T}{\Delta t}\xi_{ij}^{(\alpha)} \quad (10)$$

where the Dirac δ function is approximated by $1/\Delta t$ for the purpose of making discrete time steps.[23]

2.3. Evaluation of Excluded Volume and Bending Forces. A short-range repulsive potential maintains the excluded volume of the rods. This force acts on neighboring rods at the points of closest approach,[1,25] contributing to both the rotation and displacement of the center of mass. The forces between an interacting pair of rod segments are equal in magnitude and opposite in direction, acting along the common normal vector between the segments. Multiple repulsive forces may act on a single segment of a rod, depending on the separation distance between the surrounding fibers. The repulsive force is calculated between each segment of one rod and the two segments of every other rod in the system. The form of the repulsive potential is[5,6]

$$U^{(\mathrm{Ev})} = \frac{\varepsilon e^{-(h/\sigma)^2}}{\sin(\theta)} \quad (11)$$

where ϵ and σ are the parameters that determine the magnitude and range of the potential, $\sin(\theta)$ is the angle between the pair of interacting fibers ($|\epsilon_{ijk}p_j^{(\alpha)}p_\mathrm{k}^{(\alpha)}|$), and h is the closest distance between the center lines of a pair of fibers as calculated in the work of Frenkel and Maguire.[25] The excluded volume forces, $\mathscr{F}_i^{(\alpha,\mathrm{Ev})}$, used in eq 1 are calculated from the potential in eq 11 by taking the derivative of the potential with respect to the separation distance h. All simulations presented here used an effective aspect ratio of 50, where $\varepsilon = (50/3)k_\mathrm{B}T$ and $\sigma = 0.0771L$. These parameters for the excluded volume potential result in a short-range force which is approximately zero after a distance of about 20% of the rod length. The excluded volume potential becomes singular when the rods are perfectly parallel, and so care must be taken in the simulations in order to avoid unrealistic results.[1]

The rigidity of the rods is controlled by a bending force. The form of the bending potential is[26]

$$U^{(\mathrm{Bend})} = Kk_\mathrm{B}Tp_i^{(\alpha,1)}p_i^{(\alpha,2)} \quad (12)$$

where the stiffness parameter K sets the magnitude of the potential. The bending forces, $\mathscr{F}_i^{(\alpha,\mathrm{Bend})}$, are calculated by taking the derivative of the potential with respect to the configuration. For the simulations performed in this study, the dimensionless parameter K was set equal to 300 for rods with little bending and 10 for simulations of slightly more flexible rods.

2.4. Evaluation of Constraint and Correction Forces. Rigid constraints are placed on the rods so that the two rod segments remained attached. The constraint equations are defined as

$$g_i^{(\alpha)} = x_i^{(\alpha,1)} - x_i^{(\alpha,2)} + \frac{l}{2}(p_i^{(\alpha,1)} + p_i^{(\alpha,2)}) \equiv 0 \qquad (13)$$

for the slender-body dimer model and

$$g_a^{(\alpha)} = (x_i^{(\alpha,a+1)} - x_i^{(\alpha,a)})^2 - l^2 \equiv 0 \qquad (14)$$

for the three-bead trimer model. The constraints for the slender-body model state that the positive end of segment 1 of rod α must coincide with the negative end of segment 2. The constraints for the three-bead trimer model require that neighboring beads remain separated by a fixed distance l at all times. The first constraint ($a = 1$) of the three-bead trimer model acts between beads 1 and 2 of rod α and the second constraint ($a = 2$) acts between beads 2 and 3.

The constraint force is given by[17,22,24]

$$\mathcal{F}_i^{(\mathrm{Const})} = \lambda_j^{(\alpha)} \frac{\partial g_j^{(\alpha)}}{\partial r_i^{(\alpha)}} \qquad (15)$$

where the force is the product of the vector of Lagrange multipliers $\lambda_j^{(\alpha)}$ and the derivative of the constraints $g_j^{(\alpha)}$. The Lagrange multipliers are calculated using[15,17]

$$\dot{r}_i^{(\alpha)} \frac{\partial g_j^{(\alpha)}}{\partial r_i^{(\alpha)}} = 0 \qquad (16)$$

which requires that the rod velocities remain perpendicular to the constraints.

Once the forces acting on the rods are calculated, eq 1 is integrated in time using the midpoint method.[27,28] Naive application of rigid constraints using unmodified Brownian forces as defined in section 2.2 in conjunction with the midpoint method produces a probability distribution function which does not generally agree with kinetic theory. An additional force given by[15,16,22]

$$\mathcal{F}_i^{(\alpha,\mathrm{Corr})} = \frac{\partial^2 g_a^{(\alpha)}}{\partial r_j^{(\alpha)} \partial r_i^{(\alpha)}} \left(\frac{\partial g_a^{(\alpha)}}{\partial r_k^{(\alpha)}} \left(\xi_{kl}^{(\alpha)}\right)^{-1} \frac{\partial g_b^{(\alpha)}}{\partial r_l^{(\alpha)}} \right)^{-1} \frac{\partial g_b^{(\alpha)}}{\partial r_m^{(\alpha)}} \left(\xi_{mj}^{(\alpha)}\right)^{-1} \qquad (17)$$

is applied to correct the dynamics so that the integration procedure produces a distribution consistent with the kinetic theory for a flexible polymer model employing stiff spring forces. The correction force defined in eq 17 can be evaluated analytically as a function of the internal configuration for the models appearing in Figure 1.

2.5. Diffusivity Calculations. The simulations performed in this study ignore hydrodynamic interactions between rods and rod segments. Under this simplifying conditions, the mobility matrix for the slender-body dimer model is given by[19−21]

$$(\xi_{mn}^{(\alpha)})^{-1} = \begin{bmatrix} \delta_{ij} + p_i^{(\alpha,1)} p_j^{(\alpha,1)} & 0 & 0 & 0 \\ 0 & \delta_{ij} + p_i^{(\alpha,2)} p_j^{(\alpha,2)} & 0 & 0 \\ 0 & 0 & (12/l^2)(\delta_{ij} - p_i^{(\alpha,1)} p_j^{(\alpha,1)}) & 0 \\ 0 & 0 & 0 & (12/l^2)(\delta_{ij} - p_i^{(\alpha,2)} p_j^{(\alpha,2)}) \end{bmatrix} \qquad (18)$$

where the mobility $(\xi_{mn}^{(\alpha)})^{-1}$ has been divided by the quantity $\ln(2A)/4\pi\mu l$, where A is the aspect ratio (rod segment length l divided by rod diameter d) and μ is the viscosity of the suspending fluid. The indices m and n defining the matrix size range from 1 to 12 and the indices i and j defining the subblocks range from 1 to 3. By the definition of $\dot{r}_i^{(\alpha)}$ made in eq 2, the first two terms lying along the diagonal correspond to the center of mass mobilities of segments 1 and 2 of the slender-body dimer model and the last two blocks correspond to the rotational mobilities. The mobility matrix for the three-bead trimer model is defined as

$$\left(\xi_{mn}^{(\alpha)}\right)^{-1} = \begin{bmatrix} \delta_{ij} & 0 & 0 \\ 0 & \delta_{ij} & 0 \\ 0 & 0 & \delta_{ij} \end{bmatrix} \qquad (19)$$

where $(\xi_{mn}^{(\alpha)})^{-1}$ has been made dimensionless by dividing by the quantity $1/6\pi\mu a$, where a is the diameter of each bead. For the three-bead trimer model the indices m and n defining the matrix size range from 1 to 9 and the indices i and j are the same as with the slender-body dimer model. The upper left subblock corresponds to the center of mass mobility of bead 1, the center subblock corresponds to the mobility of bead 2, and the lower right subblock corresponds to the mobility of bead 3.

As the concentration of the semirigid rods increases, the mobility of each rod is reduced due to the excluded volume interactions with the surrounding rods. Consequently, the long-time diffusivity is altered. The long-time diffusivities are calculated from the positions and orientations of the rods over time. The average center of mass diffusivity is calculated by

$$\left\langle (x_i^{(\alpha)}(t+\tau) - x_i^{(\alpha)}(t))^2 \right\rangle = 6 D_T \tau \qquad (20)$$

for large values of τ. The brackets $\langle \cdot \rangle$ indicate an ensemble average over the time and rods α. The average center of mass position is calculated as seen in Figure 1 for each model.

To characterize the rotational dynamics of the semirigid rods, a rotational diffusion coefficient, D_R, is defined in terms of the orientation of the end-to-end vector for the rod[7,8]

$$\left\langle p_i^{(\alpha)}(t+\tau) p_i^{(\alpha)}(t) \right\rangle = \exp\left[-2 D_R \tau\right] \qquad (21)$$

where $p_i^{(\alpha)}$ is the average of $p_i^{(\alpha,1)}$ and $p_i^{(\alpha,2)}$ (see Figure 1). The overall orientation is renormalized before the diffusivities are calculated in eq 21 in order to ensure that $p_i^{(\alpha)}$ is a unit vector.

Periodic boundary conditions were used in the simulations to approximate an unbounded suspension. A cubic box of length $3.0L$ was used for the simulations for dimensionless number densities nL^3 from 50 to 150, where L is the total length of the rod. A box with sides of length $2.25L$ was used for the concentrations of $nL^3 = 200$ and 250. The number of rods simulated was determined by the size of the box and the desired number density. The various simulations used between 169 and 506 rods and used a dimensionless time-step of 1×10^{-8} for a total dimensionless simulation time of 1.0. The time-step was made dimensionless by dividing by $4\pi\mu L^3/k_B T \ln(2A)$ for the slender-body dimer model, and by $6\pi\mu a L^2/k_B T$ for the three-bead trimer model. The time-step was determined to be small enough to resolve the excluded volume forces. At the highest concentrations, the displacement caused by the repulsive forces is no more than 2% of the rod length, or $^1/_{10}$ of the interaction distance of the repulsive force. The values of the diffusivities calculated from the simulations were determined to be convergent in time by dividing the time step by two for the case of $nL^3 = 150$ for both models at either K value and the results

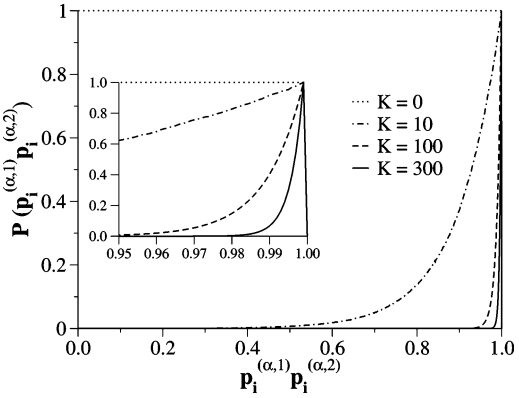

Figure 2. Probability distribution of $p_i^{(\alpha,1)}p_i^{(\alpha,2)}$ based on the value of K used for the bending force with the slender-body dimer model. The values of K used in the simulations were 10, 100, and 300. The inset is a magnification of the area where $p_i^{(\alpha,1)}p_i^{(\alpha,2)}$ is close to 1.

were equivalent. The effect of the size of the simulation box was also determined to not be a factor in the results of the simulations by increasing the size of the simulation box by 50% at the concentrations of $nL^3 = 50$ and 150 for both models.

3. Results

The following sections present the results of the simulations. First, simulations were performed of individual rods to quantify the effect of the bending forces. The results of simulations of concentrated suspensions are then presented with a study of the behavior of D_R/D_{R_0} as a function of the choice of model and the degree of rigidity of the rods. The results of the effect of bending on the translational diffusivities are also presented.

3.1. Simulations of Individual Rods. To determine the effect of bending on individual rods, studies were performed in which the magnitude of the bending force was varied. With no applied bending force ($K = 0$), the probability distribution of $p_i^{(\alpha,1)}p_i^{(\alpha,2)}$ is uniform as seen in Figure 2. The probability distribution of $p_i^{(\alpha,1)}p_i^{(\alpha,2)}$ is calculated by dividing the range of -1 to $+1$ into 200 equal sized bins, counting the number of times that the angle between the rods falls into each bin, and then normalizing the count in each bin by the largest count. The value of $p_i^{(\alpha,1)}p_i^{(\alpha,2)} = 0$ corresponds to a rod bent at 90°, while a value of $p_i^{(\alpha,1)}p_i^{(\alpha,2)} = 1$ corresponds to a straight rod. The probability distribution seen in Figure 2 approaches that of a rigid rod as the value of K increases. The inset in Figure 2 shows the quick decay of the probability distribution to zero for the rods with $K = 100$ and $K = 300$. As expected, simulations confirmed that the probability distributions for the slender-body dimer and the three-bead trimer models match.

The value of K affects the ratio of the diffusivities at infinite dilution ($L^2D_{R_0}/D_{T_0}$) for the rod models, as shown in Figure 3. The values of the ratios for each semirigid rod model have been normalized by the values for the corresponding dilute, rigid-rod models. For $K = 5$, the ratio $L^2D_{R_0}/D_{T_0}$ for the slender-body dimer model is 18.6% higher than the ratio for a rigid slender-body model. Similarly, the normalized value of the ratio for the three-bead trimer model is 9.1% higher than the ratio for a rigid trumbell. As the value of K increases from 5, the values of the ratios for the two rod models approach the values for rigid rods. The decrease in the ratio for the semirigid rod models comes from a decrease in the rotational diffusivity as the K value increases. The values of the center of mass diffusivities remain constant regardless of the value for K since hydrodynamic interactions between the rod segments are ignored.

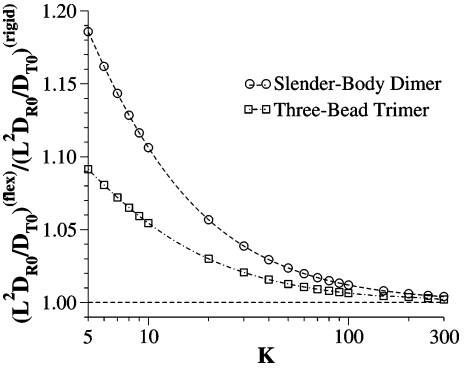

Figure 3. Values of the ratio of the dilute values of the diffusivities $L^2D_{R_0}/D_{T_0}$ resulting from the K value chosen for the magnitude of the bending force between the segments of rod α. The values of $L^2D_{R_0}/D_{T_0}$ for the semirigid rods were normalized by the rigid-rod values for each model.

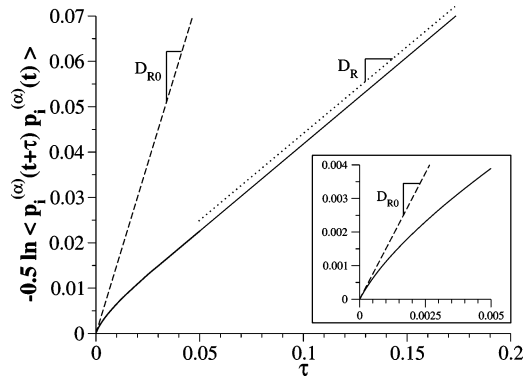

Figure 4. Plot of the orientation autocorrelation function $-0.5\ \ln\langle p_i^{(\alpha)}(t+\tau)p_i^{(\alpha)}(t)\rangle$ over time τ for the slender-body dimer model at a concentration of $nL^3 = 50$ and $K = 300$. The inset of the graph is a magnification at short times showing that D_{R_0} is recovered.

For studies of concentration effects, two different values of K were chosen. The first, $K = 300$, was chosen in order to produce rods which were nearly rigid. The second value, $K = 10$, was chosen in order to produce rods with a small degree of flexibility. The value of $K = 10$ results in a rod that is still fairly rigid, with $p_i^{(\alpha,1)}p_i^{(\alpha,2)}$ rarely falling below 0.6.

3.2. Rotational Diffusivities at High Concentrations. Systems with higher concentrations were studied using the models identified in the previous section. Figure 4 shows a plot of the autocorrelation $-0.5\ \ln\langle p_i^{(\alpha)}(t+\tau)p_i^{(\alpha)}(t)\rangle$ as a function of time τ for a suspension of slender-body dimers at a concentration of $nL^3 = 50$ and $K = 300$. The rotational diffusivity is calculated from the slope of the line after the system has come to equilibrium. For the simulations with $K = 300$ the dilute value of the rotational diffusivity is recovered at short times. The long time rotational diffusivity is then calculated from the slope of the graph at longer times.

Figure 5 shows the values of the rotational diffusivities for the models with $K = 300$ as well as for completely rigid rods. The simulations of the rigid rods were performed using the algorithm described by Cobb and Butler.[1] The rotational diffusivities for each model are normalized by the rotational diffusivities of that specific model at infinite dilution. A power-law scaling of $D_R/D_{R_0} \sim (nL^3)^\nu$ is used to compare the results of the simulations obtained in this study with the published theories.[2,3,4,7,8] The scaling calculated for the slender-body dimer model is $\nu \approx -1.95$, and the scaling for the three-bead trimer model is $\nu \approx -1.36$ over the concentrations of $nL^3 = 70$ to 150. These values for the power-law scaling are close to those of rigid rods.[1] The relative values of the rotational diffusivities

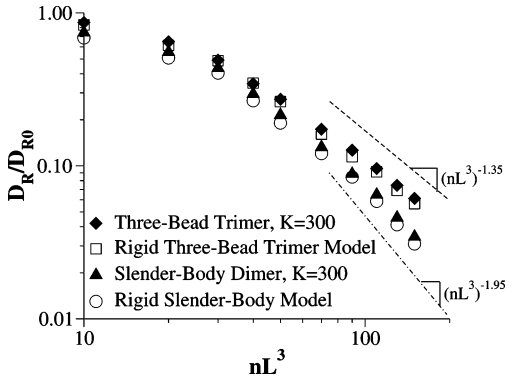

Figure 5. Rotational diffusivities of rigid slender-bodies and three-bead trumbells in comparison to the slender-body dimer and three-bead trimer models with $K = 300$. The diffusivities are normalized by their respective dilute values and are plotted as a function of the number density nL^3.

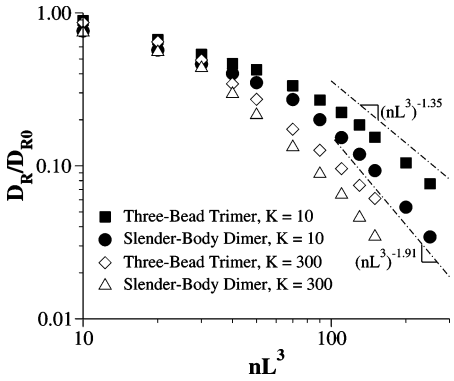

Figure 6. Rotational diffusivities of the rigid-rod models in comparison to the semirigid rod models with $K = 10$. The scaling of the semirigid rod models at concentrations greater than $nL^3 = 130$ approach that of the rigid rods.

are consistently higher for the semirigid rods, which shows that even small deviations from rigid models cause a difference. The average difference between the diffusivity values is 9.8% over the range of concentrations studied.

Over the same range of concentrations, the values of the rotational diffusivities for the more flexible rods with $K = 10$ differ significantly from the diffusivities of rigid rods. Figure 6 shows that over the range of $nL^3 = 70$ to 150, the values of D_R/D_{R_0} are higher for the simulations with the semirigid rods. The power-law scalings over this range of concentrations for the rods with $K = 10$ are $\nu \approx -1.40$ for the slender-body dimer model and $\nu \approx -1.01$ for the three-bead trimer model. The power-law fit is also not particularly good over this concentration regime, with the coefficient of determination (R^2) having a value of about 0.92 for both models. If the concentration range over which the power-law scaling is calculated is changed to $nL^3 = 130$ to 250, then the scalings approach the values for rigid rods where $\nu \approx -1.91$ for the slender-body dimer model and $\nu \approx -1.35$ for the three-bead trimer model. The power-law fit over these concentrations improves to a value of R^2 of about 0.97 for the slender-body dimer model and 0.96 for the three-bead dimer model.

The percentage error in the diffusivities calculated from the simulation results was largest at the lowest concentrations, where there were fewer rods over which to average. However, the error never exceeded 5% of the mean value for any of the diffusivity values calculated. The error bars in Figures 5 and 6 are smaller than the symbols.

3.3. Translational Diffusivities at High Concentrations. The average diffusivities of the center of mass for the rods

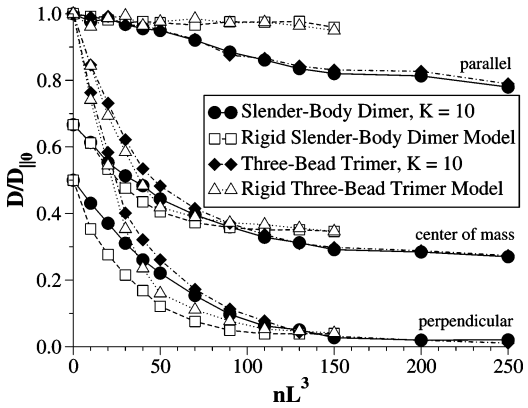

Figure 7. Translational diffusivities for the semirigid models with $K = 10$ in comparison to the diffusivities for rigid rods. The value of $D_{||}$ for the semirigid models is reduced by about 20% from the dilute value, and so lowers the overall center of mass diffusivity.

displayed in Figure 7 were calculated using eq 20. The displacements parallel and perpendicular to the central rod axis were calculated by projecting the rod center of mass displacement along the orientation over time.[1,5,6] The diffusivities of the rods with $K = 300$ are indistinguishable from the rigid rod values at all concentrations simulated. The values of $D_{||}/D_{||_0}$ are qualitatively different for models with $K = 10$ as compared to the rigid-rod models at concentrations greater than $nL^3 = 50$. The values of $D_T/D_{||_0}$ are higher for the semirigid rods with $K = 10$ up to concentrations of $nL^3 = 70$. The values of $D_T/D_{||_0}$ are lower for the semirigid rods at concentrations greater than $nL^3 = 130$. The values of $D_\perp/D_{||_0}$ are higher for the semirigid rods until about $nL^3 = 110$.

Examining the difference between the semirigid and rigid rods shows that the diffusivity parallel to the central rod axis ($D_{||}/D_{||_0}$) is reduced to about 0.8 at the highest concentrations for the rod models with $K = 10$, whereas $D_{||}/D_{||_0}$ was virtually unchanged for the rigid-rod models. This decrease in $D_{||}/D_{||_0}$ results in a reduction of the overall center of mass diffusivity at high concentrations from about 0.4 for the rigid rods to 0.3. The diffusivity perpendicular to the central rod axis is almost nonexistent at these high concentrations, where $D_{\perp_0}/D_{||_0}$ is reduced by about 97% for the slender-body dimer model and 98% for the three-bead trimer model. The perpendicular diffusivities for the slender-body dimer model at low concentrations up to $nL^3 = 90$ are smaller than the corresponding diffusivities for the three-bead dimer model for both the rigid and semirigid rod models. This difference arises from the anisotropic vs isotropic center of mass diffusivities for the slender-body dimer and three-bead trimer models, respectively. The percentage error in the center of mass diffusivity calculations was also within the 5% range, similarly to the error in the rotational diffusivities, with the error bars being smaller than the symbols in Figure 7.

4. Discussion

In comparing the simulation results of the semirigid to the rigid polymers, two main features are apparent. First, a delay in the onset of the semidilute regime is observed for the more flexible rods. Second, these semirigid rods produce the same power-law scaling for the rotational diffusivities as their corresponding rigid-rod models at sufficiently high concentrations. The origin of these two main features of the dynamics are discussed within the context of existing theories and recent simulation results.

The theories of Doi and Edwards[7] predict the onset of semidilute behavior in systems of rigid rods at lower concentra-

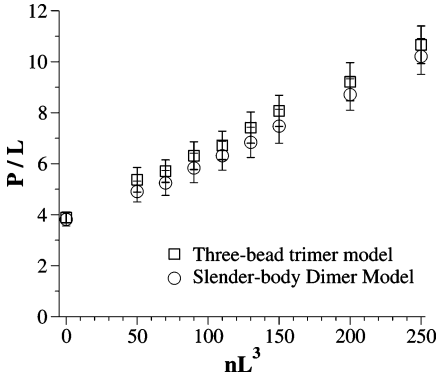

Figure 8. Ratio of the Persistence lengths (P) for the slender-body dimer and three-bead trimer models over the total rod length (L) at $K = 10$. The semirigid rods straighten on average as the concentration increases.

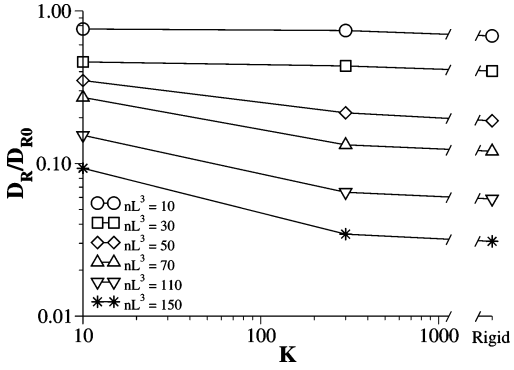

Figure 9. Rotational diffusivity as a function of the stiffness parameter K and concentration for simulations using the slender-body dimer model.

tions than observed in experiments.[29,30] The semidilute concentration regime is generally defined as the concentration at which rod rotations become sufficiently hindered to cause a marked decrease in the rotational diffusivities.[29] Keep and Pecora[8] argue that flexibility in polymers requires more blocking points (and so more rods) before the rods become caged[2] and enter the semidilute regime. The end of a flexible rod is less hindered than a rigid rod, and therefore rotates more quickly, even though the trailing portion may still be trapped. The theory of Keep and Pecora[8] states that below a critical concentration, the rods may be considered rigid when calculating the rotational dynamics. Once the system exceeds this critical concentration, effects caused by the flexibility of the rod are seen, including a delay in the onset of the semidilute concentration regime. The critical concentration is given by[8]

$$(nL^3)_{\text{crit}} = \left(\frac{418}{15\pi}\right) + \left[\left(\frac{418}{15\pi}\right)^2 + \left(\frac{768}{\pi}\right)\left(\frac{P}{L}\right)\right]^{1/2} \qquad (22)$$

where P is the persistence length, L is the total length of the rod, and $(nL^3)_{\text{crit}}$ is the concentration at which flexibility effects must be considered for polymer rod systems.

The persistence length is defined by[8]

$$\langle p_i^{(\alpha,1)} p_i^{(\alpha,2)} \rangle = \exp[-s/P] \qquad (23)$$

where s is the distance along the contour length of the rod. For the simulations performed here of semirigid rods made up of two rigid segments, the value of s is the distance along the length of the rod segments between the centers ($s = l$). In these simulations the rods have a length of $2l$ ($L = 2l$). According to the prediction of Keep and Pecora,[8] this critical concentration is where the rotational dynamics of the semirigid rods will diverge from the dynamics of rigid rods. Equation 22 predicts the critical concentration quite well for the simulations of semirigid rods with $K = 10$. Using the calculation from eq 22 along with the persistence lengths for the models at infinite dilution seen in Figure 8 produces a critical concentration of $(nL^3)_{\text{crit}} \approx 40$. Figure 6 shows the rotational diffusivities for the rigid-rod models in comparison to the semirigid rod models. The rotational diffusivities for concentrations less than $nL^3 = 30$ are equivalent, within the error of the simulations. For concentrations greater than $nL^3 = 40$, the rotational diffusivities for the models with $K = 10$ are higher than those of the rigid rods. This change in the dynamics from rigid to semirigid can be seen in a plot of the diffusivity values as a function of the stiffness parameter K used in the simulations. Figure 9 shows that for the slender-body dimer model at low concentrations, the values of D_R/D_{R_0} do not change significantly with different values of K, or for the rigid models. As the concentration increases, the rigid models and models with high bending stiffness have much lower rotational diffusivity values than the models with $K = 10$. The rotational diffusivity values for the three-bead trimer model produce a result which is qualitatively similar to that of Figure 9.

The second major observation of the dynamics of rod suspensions is the similarity in the power-law scaling between the rigid and semirigid rod models. The rotational diffusivities seen in Figure 6 show that as the concentration increases up to $nL^3 = 250$, the power-law scalings of D_R/D_{R_0} approach the values for rigid rods. This would seem to indicate that the semirigid rods behave as fully rigid rods at sufficiently high concentrations. To study the onset of rigid-rod like behavior as a function of concentration, the persistence length of the rods was calculated from the simulation data as a function of concentration. The rigidity of the rod is related to the ratio of the persistence length to the length of the rod (P/L). A completely straight rod will have a ratio of $P/L = \infty$. Figure 8 shows the persistence length ratios of the semirigid rods with $K = 10$ as calculated in eq 23. The persistence length ratios for these semirigid rods vary between $P/L = 3.9$, corresponding to an average angle between the rods of about 39 degrees from a straight conformation, and $P/L = 10.7$, corresponding to an angle of about 24°, over the range of concentrations studied. A value of $P/L = 10$ (average angle of about 25° from rigid), is considered to be very stiff.[8] Figure 8 also shows that the persistence length increases with increasing concentration. This increase demonstrates that the rods spend more time in a straight, or rigid conformation as the concentration increases. Once the configuration of the rods becomes straight enough due to caging, the rotational diffusivity begins to decrease with nearly the same power-law scaling as the corresponding rigid model. The power-law scaling for the rotational diffusivities of the semirigid slender-body dimer model with $K = 10$ at concentrations higher than $nL^3 = 110$ is almost identical to the power-law scaling of the rigid-slender body model at concentrations greater than $nL^3 = 70$. The same is true for the power-law scaling of the semirigid three-bead trimer model in comparison to the rigid three-bead trumbell model over the same concentration regime.

The power-law scaling values are different for each hydrodynamic model, as expected from recent simulation work.[1] Theories for the scaling of the rotational diffusivities of rod systems in solution have existed in the scientific literature for many years, with the earliest theories based on systems of rigid rods with high aspect ratios.[2−4] The power-law scaling of $D_R/D_{R_0} \sim (nL^3)^{-2}$ predicted by the theories and simulations of Doi

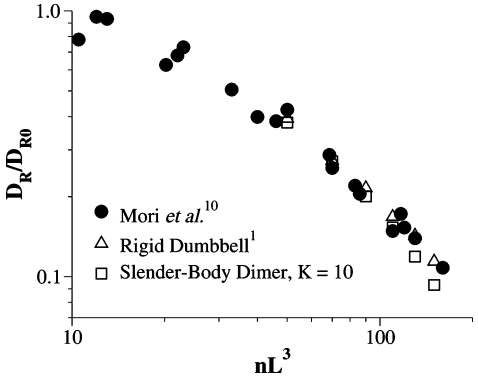

Figure 10. Rotational diffusivities of the slender-body dimer with $K = 10$ in comparison to simulations of a rigid-dumbbell,[1] and the rotational diffusivities measured by Mori et al.[10] in systems of PBLG.

and Edwards[7] have been reported to be incorrect based on simulation results.[3,4] Disagreements concerning the observed power-law scaling have been shown to originate with the choice of hydrodynamic model used within the simulations.[1] The power-law scaling predicted by Doi and Edwards[7] is, however, observed in many experiments.[8]

As a note about the scalings, the use of a power-law scaling to characterize the rotational dynamics of polymer rod systems at high concentrations has not been rigorously justified.[31,1] In fact, the agreement between the simulation data and the power-law fits is not particularly convincing; relatively few points are used to calculate the exponent ν, and the correlation is not particularly good. However, in keeping with the literature on the subject of rotational diffusivity of polymer rods, a power-law fit of the simulation data is used to provide a convenient way of collapsing all of the data for the rotational diffusivities in the semidilute concentration regime into a single number, which can be then readily compared to existing theories.

The rotational diffusivities for the slender-body dimer rods with $K = 10$ are shown in Figure 10 in comparison to the experimental findings of Mori et al,[10] as well as simulations of rigid-dumbbells by Cobb and Butler.[1] Some researchers have claimed that the $\nu = -1$ scaling measured in the experiments of Mori et al[10] over this intermediate concentration regime show that the rigid-dumbbell model should be used in simulations of polymer rods because it reproduces the experimental results well.[5,6] The results in Figure 10 show that simulations of semirigid slender-body dimers will also reproduce the rotational diffusivity results of Mori[10] over this range of concentrations. Consequently, the degree of flexibility and hydrodynamic model cannot be uniquely determined on the sole basis of a comparison between the measured and calculated rotational diffusivities for this intermediate range of concentrations. By comparing with experiments at higher concentrations, distinguishing between the two effects of flexibility and hydrodynamic model should be possible.

Flexibility also noticeably impacts the center of mass diffusion of the semirigid rods. Doi and Edwards[7] predict that the concentration dependence of the average center of mass diffusivity decreases for increasingly flexible rods. The drop in the average center of mass diffusivity, as seen in Figure 7, confirms the accuracy of the prediction. This decrease in the parallel diffusivity is caused by the fact that when the rod is bent, the motion parallel to the central axes of each segment does not translate completely into the motion along the overall orientation of the rod as a whole. A bent rod will travel along its parallel direction through a tube less freely than a rigid rod.

5. Conclusions

Simulations of models incorporating a small degree of flexibility can provide a simple, yet valuable insight into the dynamics of rod suspensions. The degree of flexibility and the type of hydrodynamic model chosen have a dual effect on the rotational diffusivities of rod systems. The flexibility of the rods becomes important above a critical concentration, where it causes a delay in the onset of the semidilute concentration regime. The degree of flexibility does not however change the value of ν in the power-law scaling of $D_R/D_{R_0} \sim (nL^3)^\nu$ at high concentrations for that specific hydrodynamic model. Instead the flexibility simply increases the concentration at which the scaling is observed. The choice of hydrodynamic model used to represent the rods in the simulations has a significant impact on the value of ν in the power-law scaling at high concentrations.

Different micromechanical models have been shown to be able to reproduce experimental results. The rods simulated here are not completely realistic in comparison to actual experimental polymer rods since the important effect of multibody hydrodynamic interactions have not been taken into account. The hydrodynamic interactions will alter the short-time dynamics of the rods and, consequently, the long-time diffusivities. The simulation results can be used as a tool to obtain qualitative comparisons to experimental systems and also as a reference to compare to simulations in which multibody hydrodynamic interactions are included.

Acknowledgment. This research project was supported by the National Science Foundation through a CAREER Award (CTS-0348205).

References and Notes

(1) Cobb, P. D.; Butler, J. E. *J. Chem. Phys.* **2005**, *123*, 054908.
(2) Doi, M.; Yamamoto, I.; Kano, F. *J. Phys. Soc. Jpn.* **1984**, *53*, 3000−3003.
(3) Fixman, M. *Phys. Rev. Lett.* **1985**, *54*, 337−339.
(4) Fixman, M. *Phys. Rev. Lett.* **1985**, *55*, 2429−2432.
(5) Bitsanis, I.; Davis, H. T.; Tirrell, M. *Macromolecules* **1988**, *21*, 2824−2835.
(6) Bitsanis, I.; Davis, H. T.; Tirrell, M. *Macromolecules* **1990**, *23*, 1157−1165.
(7) Doi, M.; Edwards, S. F. In *The Theory of Polymer Dynamics*; Oxford University Press: Oxford, U.K., 1986.
(8) Keep, G. T.; Pecora, R. *Macromolecules* **1988**, *21*, 817−829.
(9) Cush, R. C.; Russo, P. S. *Macromolecules* **2002** *35*, 8659−8662.
(10) Mori, Y.; Ookubo, N.; Hayakawa, R.; Wada, Y. *J. Polym. Sci., Polym. Phys. Ed.* **1982**, *20*, 2111.
(11) Tracy, M. A.; Pecora, R. *Annu. Rev. Phys. Chem.* **1992**, *43*, 525−557.
(12) Phalakornkul, J. K.; Gast, A. P.; Pecora, R. *Macromolecules* **1999**, *32*, 3122−3135.
(13) Van Bruggen, M. P. B.; Lekkerkerker, H. N. W.; Dhont, J. K. G. *Phys. Rev. E* **1997**, *56*, 4394−4403.
(14) Van Bruggen, M. P. B.; Lekkerkerker, H. N. W.; Maret, G.; Dhont, J. K. G. *Phys. Rev. E* **1998**, *58*, 7668−7677.
(15) Butler, J. E.; Shaqfeh, E. S. G. *J. Chem. Phys.* **2005**, *122*, 014901.
(16) Butler, J. E. *J. Fluid Mech.* **2005**, submitted for publication.
(17) Hinch, E. J. *J. Fluid Mech.* **1994**, *271*, 219−234.
(18) Yu, H.; Stockmayer, W. H. *J. Chem. Phys.* **1967**, *47*, 1369−1373.
(19) Batchelor, G. K. *J. Fluid Mech.* **1970**, *44*, 419−440.
(20) Cox, R. G. *J. Fluid Mech.* **1970**, *44*, 791−810.
(21) Cox, R. G. *J. Fluid Mech.* **1971**, *45*, 625−657.
(22) Morse, D. C. *Adv. Chem. Phys.* **2004**, *128*, 65−189.
(23) Ottinger, H. C. *Rheol. Acta* **1996**, *35*, 134−138.
(24) Klaveness, E.; Elgsaeter, A. *J. Chem. Phys.* **1999**, *110*, 11608.
(25) Frenkel, D.; Maguire, J. F. *Mol. Phys.* **1983**, *49*, 503−541.
(26) Pasquali, M.; Shankar, V.; Morse, D. C. *Phys. Rev. E* **2001**, *64*, 020802.
(27) Fixman, M. *J. Chem. Phys.* **1978**, *69*, 1527−1537.
(28) Grassia, P. S.; Hinch, E. J.; Nitsche, L. C. *J. Fluid Mech.***1995**, *282*, 373−403.
(29) Odjik, T. *Macromolecules* **1983**, *16*, 1340−1344.
(30) Thirumalai, D. *J. Phys. Chem.* **1994**, *98*, 9265−9269.
(31) Keep, G. T.; Pecora, R. *Phys. Rev. Lett.* **1985**, *18*, 1167−1173.

MA052164B